Strategies for Non-Linear Deformation Estimation from Interferometric Stacks

B.M. Kampes, R.F. Hanssen, L.M.Th. Swart
Delft University of Technology
Thijsseweg 11, 2629 JA Delft, The Netherlands

Abstract— **A testing procedure is presented to estimate topography and deformation parameters from an interferometric stack (a number of reference phase corrected interferograms w.r.t. the same master image). A subset of pixels exhibit coherent phase in time, and a time series of phase differences between pairs of these pixels allows to set up a system of equations. A null hypothesis of zero deformation can be tested against alternative hypotheses, specifying linear and non-linear deformation. The covariance matrix of the phase differences accounts for phase noise, atmospheric effects, and orbit inaccuracies.**

I. Introduction

Spaceborne repeat-pass interferometric SAR (InSAR) has been recognized over the last decade as a valuable technique for deformation studies. Spectacular results have been obtained, e.g., showing the 2D deformation pattern after earthquakes, or the inflation and deflation of volcanos. However, many of these studies have been rather opportunistic: the deformation phenomena have a large signal, are spatially limited, or occur over a short time interval, while the observed areas remain relatively coherent in time and have minimal atmospheric variation. In these circumstances, successful results are almost guaranteed.

In (more frequently occurring) non optimal situations, where a small deformation signal needs to be detected amidst atmospheric disturbances and temporal decorrelation, the standard differential processing of a small number of images generally yields much poorer results, resulting in a highly decorrelated and biased interferogram. To use InSAR in those situations more advanced approaches of the problem are inevitable.

Here we use stacks of interferograms, preferably utilizing all available radar acquisitions. Instead of analyzing these interferograms in the traditional 2D manner we search for individual pixels that have consistent phase statistics in time (1D). We follow the concept of the recently introduced "permanent scatterers technique", see [1]. To identify the consistent pixels this method typically requires a large number of images and a priori assumptions on the deformation characteristics. We present a methodology to test alternative hypotheses against a null hypothesis for different deformation models, e.g., linear vs. seasonal dependent, and to use the distance between pixel pairs to derive a priori variances to account for atmospheric disturbances. In the experimental section of this paper the proposed methodology is validated using a simulation.

II. Method

In this section we first derive the equations for reference phase corrected interferometric phase differences between two pixels. These phase differences can be regarded as observations, containing information on the topographic and deformation difference. The other contributions to this phase, such as atmospheric delays, are moved to the stochastic model. We assume we have $N+1$ Single Look Complex (SLC) images, or a stack (datacube) of N interferograms w.r.t. a master image at time $t=0$.

In Fig. 1 the geometric configuration and notation is shown. Sub-indices indicate time (or acquisition number, which is equivalent); the number 0 is used for the master image. A superscript ^{0} indicates a relation with the reference body, for example an ellipsoid or DEM. The phase is denoted with ϕ, and the reference corrected phase by ν. The far-field approximation is used where appropriate, assuming parallel range vectors.

The phase in SLC image i, for pixel P, at $t=i$ is defined by

$$\phi_i = -\frac{4\pi}{\lambda} r_i + \phi_{\mathrm{o}_i} + \phi_{\mathrm{A}_i} + \phi_{\mathrm{n}_i}, \tag{1}$$

where $r_i = r_0 + \Delta r_i - B\sin(\theta-\alpha)$, r_0 is the range to the master satellite, Δr_i is the deformation along the line of sight, ϕ_{o_i} indicates the scattering characteristics, ϕ_{A_i} the phase due to atmospheric delays, and ϕ_{n_i} the noise. The reference phase for the same pixel P is defined as

$$\phi_i^0 = -\frac{4\pi}{\lambda} r_i^0, \tag{2}$$

where r_i^0 is the range from the satellite position at $t=i$ to the reference point P^0 located at the reference body at a distance r_0 to the master spacecraft, such that the range vector is zero-Doppler. The phase of SLC image i, corrected for the reference, is denoted by $\nu_i = \phi_i - \phi_i^0$. The interferometric phase w.r.t. the master image corrected for the phase of a reference body is

$$\begin{aligned}
\nu_{0i} &\doteq \nu_0 - \nu_i \\
&= -\frac{4\pi}{\lambda}\left(B_\parallel - B_\parallel^0 - \Delta r_i\right) + \phi_{\mathrm{o}_{0i}} + \phi_{\mathrm{A}_{0i}} + \phi_{\mathrm{n}_{0i}} \\
&= -\frac{4\pi}{\lambda}\left(-B_\perp^0\,\delta\theta - \Delta r_i\right) + \phi_{\mathrm{o}_{0i}} + \phi_{\mathrm{A}_{0i}} + \phi_{\mathrm{n}_{0i}} \\
&= -\frac{4\pi}{\lambda}\frac{B_\perp^0}{r_0\sin\theta^0}h - \frac{4\pi}{\lambda}\Delta r_i + \phi_{\mathrm{o}_{0i}} + \phi_{\mathrm{A}_{0i}} + \phi_{\mathrm{n}_{0i}}
\end{aligned}$$

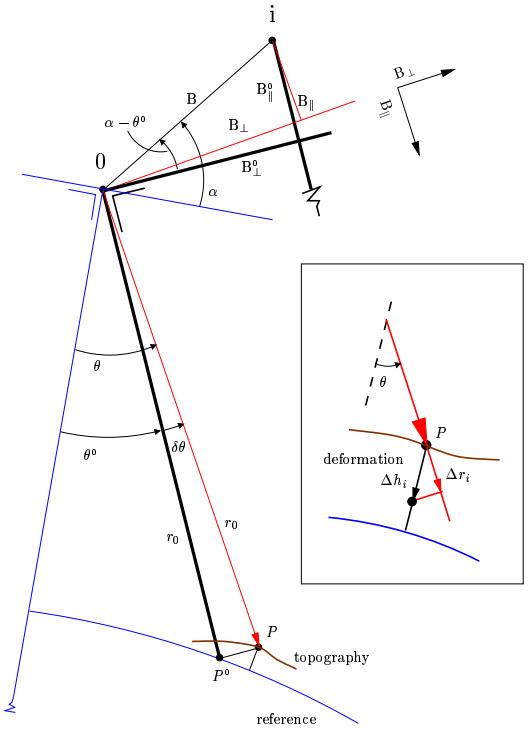

Fig. 1. Geometric configuration and definition of symbols. All angles are defined counterclockwise. The terrain element P corresponding to the radar coordinate (azimuth, range) is located at a height h above the reference body at $t = t_0$. The inset shows that at $t = t_i$ the point P can be deformated by Δh_i, with its projection on the direction of the line of sight Δr_i (positive direction same as $B_\parallel$). Note that the angles are exaggerated and the baselines magnified. The angle $\delta\theta$ is approximately 1° for an elevation of 5 km for ERS satellites.

$$= \quad \nu_{\mathrm{T}0i} + \phi_{\mathrm{D}0i} + \phi_{\mathrm{o}_{0i}} + \phi_{\mathrm{A}_{0i}} + \phi_{\mathrm{n}_{0i}} \tag{3}$$

($B^0_\parallel - B_\parallel = \delta\theta B^0_\perp$ can be easily derived geometrically from Fig. 1.) Topography is included in this expression by rewriting $\delta\theta$ ($h = r_0(\cos\theta^0 - \cos\theta) = -2r_0[\sin((\theta^0 - \theta)/2)\sin((\theta^0 + \theta)/2)] \approx r_0\delta\theta\sin\theta^0$).

Obviously, radar interferometry only works if the scattering characteristics remain more or less equal for $t = \{0, i\}$, i.e., $\phi_{\mathrm{o}_{i0}} \approx 0$ in (3), which implies low temporal decorrelation. This condition is in general only satisfied for a small subset of all pixels, resulting in a noisy interferogram. This subset can be referred to as "permanent scatterers". A part of this subset can be identified based on a time series of the amplitude values, see [1], [2]. The problem is to estimate topography and deformation of this subset.

The noise term in (3) should be small, as well as the atmospheric difference. The expectation of the latter term is zero, but its variance can be significant, depending on the water vapor distribution during the two acquisition [3].

A. Phase differences

Considering phase differences between nearby pixels–for which temporal decorrelation is limited–has the advantage that the atmospheric phase difference term decreases due to its strong spatial correlation. The same is true for errors in the computed reference phase based on precise orbits. The notation (x_1, x_2) is used to indicate the difference between two pixels in the interferograms. The following expression is valid for the interferometric phase difference

$$\begin{aligned}\nu^{\mathsf{W}}_{0i}(x_1,x_2) &= \mathsf{W}\{\nu^{\mathsf{W}}_{0i}(x_1) - \nu^{\mathsf{W}}_{0i}(x_2)\} \\ &= \nu_{\mathrm{T}\,0i}(x_1,x_2) + \phi_{\mathrm{D}\,0i}(x_1,x_2) + \\ &\quad \phi_{\mathrm{o}_{i0}}(x_1,x_2) + \phi_{\mathrm{A}_{i0}}(x_1,x_2) + \phi_{\mathrm{n}_{i0}}(x_1,x_2) - \\ &\quad k_{0i}(x_1,x_2)\cdot 2\pi, \end{aligned} \tag{4}$$

where the topography and deformation terms are

$$\nu_{\mathrm{T}}(x_1,x_2) = \frac{4\pi}{\lambda}\,\frac{B_\perp(x)}{r_0(x)\sin\theta_x}(h_{x_1} - h_{x_2}), \tag{5}$$

$$\phi_{\mathrm{D}}(x_1,x_2) = \frac{4\pi}{\lambda}\,[\Delta r_{0i}(x_1) - \Delta r_{0i}(x_2)]\,. \tag{6}$$

The phase of the complex interferogram is wrapped, denoted by the superscript $^{\mathsf{W}}$. The ambiguities $k_{0i}(x_1,x_2) \in \mathbb{Z}$ are defined such that $\nu^{\mathsf{W}}_{0i}(x_1,x_2)$ lies in the principal interval $[-\pi,\pi)$. At this point we also would like to model the deformation along the line of sight as a function of time, e.g., as linear deformation

$$\Delta r_t(x) = T_t \cdot \mu_x. \tag{7}$$

The temporal baseline is defined as $T_i = (t_i - t_0)/365$ (t_i as day number since some reference). However, depending on the driving mechanism of the deformation, it can also be modeled as, e.g., a linear part and a part with a period of 1 year, with a maximum in winter:

$$\Delta r_t(x) = T_t\mu_{1_x} + [\cos(2\pi(T_t - \Delta t)) - \cos(2\pi\Delta t)]\mu_{2_x}, \tag{8}$$

where μ_{2_x} is the amplitude of the seasonal term, and Δt is the shift of t_0 to January 1st, i.e., the maximum deformation is at time $t_0 + \Delta t$. It is noted that in order to estimate this term, the sampling in time should be dense enough. The number of parameters for the deformation model is denoted by d. These equations can be written in matrix notation as

$$\mathsf{E}\{\nu^{\mathsf{W}}\} = \begin{bmatrix} T & D & | & I \end{bmatrix} \cdot \begin{bmatrix} h_{x_1x_2} \\ \mu_{x_1x_2} \\ -- \\ k \end{bmatrix}; \qquad \mathsf{D}\{\nu\} = Q_\nu, \tag{9}$$

where the observations are the interferometric, reference corrected, phase differences between locations x_1 and x_2 at times $t = 1, ..., N$; vector T $(N \times 1)$ defines the influence of topography on the observed phase difference, see (5), and D $(N \times d)$ the influence of deformation according to a model (e.g., (7)), see (6). I is the identity matrix scaled by 2π. The unknown parameters are the topographic difference and d deformation parameter(s), and the integer

ambiguities k_{0j} in vector k $(N \times 1)$. The dispersion matrix of the observations is a full matrix $(N \times N)$. In this matrix atmospheric noise, orbit errors, and phase noise is accounted for. The full covariance matrix for the interferometric phases can be written as the sum of a diagonal matrix, accounting for the usual phase noise, and a full matrix, accounting for the atmospheric covariances. The atmospheric part can be computed from a covariance function based on the distance between locations x_1 and x_2 [3]. For our purpose, this matrix then must be propagated for the difference between locations, yielding Q_ν. Note that if the variance of the interferometric phase is σ^2 then that of the phase difference is $2\sigma^2$, assuming equal accuracies.

We would like to solve the above equation for topography and deformation, but this seems impossible. For each observation we have an unknown ambiguity, besides the parameters for topography and deformation. In general such a system cannot be solved; there are more unknowns than observations. However, usually we have extra information. First, we know that the ambiguities are integers, which reduces the solution space. Second, we can limit the solution space by introducing maximum values for the topographic and deformation differences. This leads to the following algorithm:

1. Obtain maximum values for the unknown topography and deformation parameters.
2. With these maxima, compute a (large) number of unique sets of ambiguities, such that the solution space is sampled properly. (Each set represents a certain unwrapping attempt, which can be regarded as an alternative hypothesis.)
3. For each set, unwrap the data with these ambiguities and assume as null hypothesis $H_0 : \mathsf{E}\{\nu\} = T \cdot h_{x_1 x_2}$, i.e., no deformation. Test the null hypothesis against several alternative hypotheses. The DIA testing procedure is [4]:

Detection Test the overall validity of the null hypothesis with the overall model test (OMT, see (13)). If the null hypothesis is accepted, use this estimate for the topographic difference. Else, continue with the identification step.

Identification If the null hypothesis is rejected, possible model misspecifications need to be identified. Compute the OMT for all alternatives that are accepted. It is standard practise in geodesy to always first check the individual observations for potential blunders (data snooping). Since we already check different ambiguity sets, these conventional alternative hypotheses are not considered in this step. The first alternative hypothesis is an extension of the model with linear deformation $H_A : \mathsf{E}\{\nu\} = T h_{x_1 x_2} + D\mu_1$. The second alternative hypothesis that is tested is that linear and seasonal deformation occurs. Other alternative hypotheses could be tested, for example specifying breakpoints where linear deformation starts. The (accepted) alternative hypothesis with the best OMT test statistic is regarded to have identified the model errors.

Adaption If the model misspecifications have been identified, the null hypothesis is replaced by that alternative hypothesis. The overall validity of this model needs to be detected again, and, if rejected, the stochastic model may be relaxed, since an estimate for the variance factor is given as $\hat{\sigma} = \mathrm{OMT}/(m-n)$. As a final step data snooping can be performed.

B. Hypotheses Testing

The correctness of a model of observation equations may be verified by several hypothesis tests. The null hypothesis reads $H_0 : \mathsf{E}\{y\} = Ax$, with A the full rank $m \times n$ design matrix, and x the vector of parameters. An alternative hypothesis is specified as $H_A : \mathsf{E}\{y\} = Ax + C\nabla$, where ∇ is some $q \times 1$ bias vector, and C a $m \times q$ matrix specifying the test. $[A|C]$ needs to be of full rank [4]. This means that we must have a suitable distribution of interferograms over time and space. If for example the perpendicular baseline for all images would be zero meters, topography cannot be estimated. The general expression for the test statistic is

$$T_q = \epsilon^T Q_y^{-1} C \left[C^T Q_y^{-1} Q_{\hat{\epsilon}} Q_y^{-1} C \right]^{-1} C^T Q_y^{-1} \epsilon, \tag{10}$$

where ϵ is the vector of least squares corrections with covariance matrix $Q_{\hat{\epsilon}}$. The (unwrapped) observables are assumed to be normally distributed, in first order approximation, which implies that the test statistic has a χ^2 distribution

$$H_0 : T_q \sim \chi^2(q, 0); \quad H_A : T_q \sim \chi^2(q, \lambda), \tag{11}$$

where $\lambda = \nabla^T C^T Q_y^{-1} Q_{\hat{\epsilon}} Q_y^{-1} C \nabla$ is the non-centrality parameter. The null hypothesis is rejected if

$$T_q > \chi^2_\alpha(q, 0), \tag{12}$$

with $\chi^2_\alpha(q, 0)$ the critical value, and α the level of significance (probability that H_0 is falsely rejected). If the alternative hypothesis is accepted, this is however no proof that this model is correct. The most common tests in geodetic practise are the test for blunders in individual observations (w tests) and and the overall model test (OMT). For the first type of test, the C matrix is $[0, ..., 0, 1, 0, ..., 0]^T$, where the 1 is at the ith position when we test for a blunder in the ith observation. If all observations are systematically tested this way, it is referred to as data snooping. For a diagonal covariance matrix, this test reduces to $w_i = \hat{\epsilon}_i / \sigma_{\hat{\epsilon}_i}$. For the OMT, matrix C does not need to be specified. It gives an indication of the validity of H_0. This test statistic is given as

$$T = \epsilon^T Q_y^{-1} \epsilon. \tag{13}$$

III. Experiment

In this section we validate the proposed testing procedure by means of a simulation. The configuration of the acquisitions is shown in Fig. 2, where we assumed 19 interferograms, with perpendicular baselines between -868 and 761 meters, and temporal baselines between -3.7 and 4.4 years. For a pair of pixels, approximately 2 km apart, we have simulated noisy observations for the phase difference for each interferogram. Three input parameter sets $\{h_{x_1 x_2}, \mu_1, \mu_2\}$ were used: {10, 0, 0}, {10, 10, 0}, and {10,

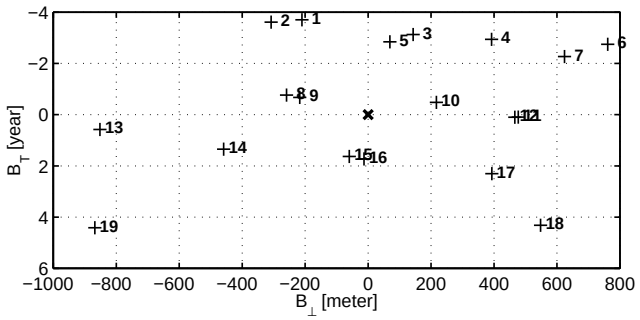

Fig. 2. Interferogram distribution relative to master SLC (×). The location of the interferogram is given as function of temporal baseline on the vertical axis and perpendicular baseline on the horizontal axis.

10, 10}. The noise standard deviation for the phase difference was set to 20, 30, 40, and 50 degrees. This corresponds to coherence levels of 0.99, 0.97, 0.95, and 0.92. Covariances are not taken into account. For each noise level, 100 simulations have been performed, estimating the parameters according to the testing procedure. Maximum values to limit the search were set to 20 m for topography and 20 mm/year for the deformation parameters.

The estimates that were accepted are plotted in Fig. 3 for these three cases. Evidently, the procedure works better for a small standard deviation. For these noise levels, only in a very small number of cases the wrong model was accepted, and in those cases the estimates for the deformation parameters were close to zero (the "true" value).

Table I shows for each case the number of times the OMT was accepted, although the wrong ambiguities were found. The total number of times the OMT was rejected is given in parentheses. For large standard deviations, the null hypothesis is often falsely accepted. This imposes limitations on the maximum allowable standard deviation of the phase observations, in order to retrieve the correct ambiguities and the topography and deformation parameters.

IV. Conclusions

A three step testing procedure is presented to estimate topographic and deformation parameters from an interferometric stack. The significance of alternative hypotheses specifying deformation models against a null hypothesis of zero deformation can be tested. The procedure consists of Detection, where the overall validity of the null hypothesis is tested; Identification, where the model misspecifications are identified if the null hypothesis was rejected; and Adaption, where the null hypothesis is replaced by the identified alternative hypothesis.

It has been shown by simulation that with this procedure non-linear deformation can be identified between pairs of pixels, provided that the noise level is limited.

TABLE I

Falsely accepted and total rejected OMTs for the three testcases.

case \ σ	20	30	40	50
1	0 (33)	0 (51)	5 (46)	84 (0)
2	0 (46)	0 (59)	0 (70)	83 (0)
3	0 (33)	0 (47)	7 (68)	31 (52)

For each case, 100 simulations have been performed for 4 levels of phase noise. Given is the number of accepted OMTs, for which the wrong ambiguities are recovered. In parentheses the total number of rejected OMTs is given.

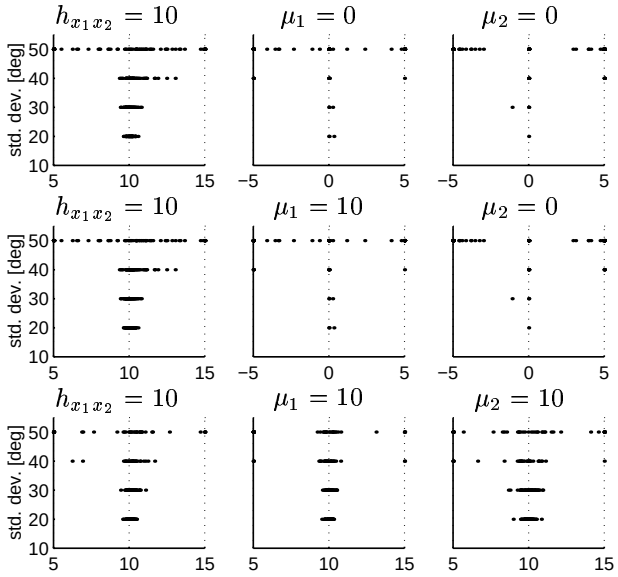

Fig. 3. Simulation results. Plotted is the distribution of 100 estimated topography and deformation parameters as function of input noise level. The input parameter values are centered at the horizontal axis for the three cases (from left to right $h_{x_1x_2}, \mu_1, \mu_2$).

References

[1] A. Ferretti, C. Prati, and F. Rocca, "Nonlinear subsidence rate estimation using permanent scatterers in differential SAR interferometry," *IEEE Trans. Geosci. Remote Sensing*, vol. 38, no. 5, pp. 2202–2212, Sep. 2000.

[2] A. Ferretti, C. Prati, and F. Rocca, "Permanent scatterers in SAR interferometry," *IEEE Trans. Geosci. Remote Sensing*, vol. 39, no. 1, pp. 8–20, Jan. 2001.

[3] R.F. Hanssen, *Radar Interferometry: Data Interpretation and Error Analysis*, Kluwer Academic Publishers, Dordrecht, 2001.

[4] P.J.G. Teunissen, *Testing theory; an introduction*, Delft University Press, Delft, 1 edition, 2000.